Chinese Chemical Letters 37 (2026) 110956

Contents lists available at ScienceDirect

Chinese Chemical Letters

journal homepage: www.elsevier.com/locate/cclet

Synergistic anti-inflammatory effect of cascade nanozymes for neural recovery in ischemic stroke

Chenchen Xie[a,1], Jun Liao[b,1], Yi Li[a,1], Yunan Zhang[a], Zhicheng Xiao[a], Yun Wang[a], Ting Chen[a], Liyan Xiong[a], Tao Pang[c], Xiangao Jiang[d], Feng Zhang[c,*], Chuan Zhang[a,*], Tingfang Wang[a,*]

[a] 411 Hospital of Shanghai University, School of Medicine, Shanghai University, Shanghai 200444, China
[b] Beijing Key Laboratory of Tumor Systems Biology, Institute of Systems Biomedicine, School of Basic Medical Sciences, Peking University, Beijing 100191, China
[c] Department of Pharmacy, Changzheng Hospital, Naval Medical University, Shanghai 200003, China
[d] Department of Infectious Disease, Wenzhou Central Hospital, Dingli Clinical College of Wenzhou Medical University, Wenzhou Sixth People's Hospital, Wenzhou 325000, China

ARTICLE INFO

Article history:
Received 4 December 2024
Revised 12 February 2025
Accepted 13 February 2025
Available online 15 February 2025

Keywords:
Ischemic stroke
Nanozymes
Reactive oxygen species
Blood-brain barrier
Neuroprotection

ABSTRACT

Overproduction of reactive oxygen species (ROS) following ischemic injury triggers an inflammatory response, significantly impeding neurological functional recovery. Nanozymes with potent antioxidative and anti-inflammatory effects thus offer great potential for ischemic stroke treatment. In this study, we developed an ischemia-homing nanozyme by combining melatonin (MT)-loaded honeycomb manganese dioxide (MnO_2) nanoflowers with M2-type microglia membranes to rescue the ischemic penumbra. The surface-engineered M2-type microglia membranes provided intrinsic ischemia-homing and blood-brain barrier (BBB)-crossing properties to the biomimetic nanozymes. This nanozyme can not only transforms harmfulsuperoxide anion radicals ($^{\bullet}O^{2-}$) and hydrogen peroxide (H_2O_2) into harmless water and oxygen but also scavenges highly toxic hydroxyl radicals ($^{\bullet}OH$), dramatically lowering intracellular ROS levels. More importantly, the biomimetic nanoparticles reduce cerebral infarct areas and provide significant neuroprotection against ischemic stroke by lowering oxidative stress, inhibiting cell apoptosis, and decreasing inflammation. This study may offer a viable approach for the use of nanozymes in treating ischemic stroke.

© 2025 Published by Elsevier B.V. on behalf of Chinese Chemical Society and Institute of Materia Medica, Chinese Academy of Medical Sciences.

Stroke is one of the most prevalent cerebrovascular diseases worldwide, resulting in considerable disability and high mortality rates [1]. Ischemic stroke, accounting for approximately 80% of all strokes, occurs when a blood vessel becomes occluded [2]. The standard approach to treating ischemic stroke involves the administration of tissue plasminogen activator (tPA) to dissolve blood clots and restore blood flow [3]. However, the use of thrombolytic therapy is severely limited due to the narrow time window for effective intravenous administration [4]. Thrombolysis or thrombectomy beyond the therapeutic window increases the risk of disruption of the blood-brain barrier (BBB), which can cause neuronal damage and functional impairment, resulting in reperfusion injury. Moreover, many therapeutic agents, including edaravone [5] and butylphthalide [6], face significant challenges in crossing the BBB, limiting their effectiveness in treating brain disorders [7,8]. Therefore, it is critical to discover new drug delivery systems that target the pathophysiology of ischemic stroke and overcome the BBB barrier.

Reperfusion can lead to an overproduction of reactive oxygen species (ROS), including superoxide anion ($^{\bullet}O^{2-}$), hydroxyl radical ($^{\bullet}OH$), and H_2O_2 [9–12]. Excess ROS induces oxidative stress, resulting in neuronal necrosis or apoptosis by oxidizing bio-macromolecules and triggering the apoptotic pathways [10–13]. Scavenging excess ROS has been shown to slow the process of neuronal death and improve prognosis [14]. Recent research has focused on oxygen delivery carriers *in vivo*. However, systemic oxygen carriers, such as hemoglobin-based oxygen carriers, suffer from low brain-targeted oxygen release efficiency [15,16]. Consequently, exploring innovative drug delivery platforms to remove excess ROS during ischemia-reperfusion and crossing the BBB barrier is crucial. Recently, nanodrug delivery systems have

* Corresponding authors.
E-mail addresses: fengzhang@smmu.edu.cn (F. Zhang), zc843016@shu.edu.cn (C. Zhang), wangtf66@shu.edu.cn (T. Wang).
[1] These authors contributed equally to this work.

https://doi.org/10.1016/j.cclet.2025.110956
1001-8417/© 2025 Published by Elsevier B.V. on behalf of Chinese Chemical Society and Institute of Materia Medica, Chinese Academy of Medical Sciences.

shown potential for future therapeutics, particularly biomimetic nanodrug delivery systems encapsulating cell membranes [17]. The natural features acquired from cells help nanoparticles minimize immunogenicity and extend half-life [18]. Microglia are activated after ischemia and exist in two different functional phenotypes: pro-inflammatory M1 and anti-inflammatory M2 [19–22]. It has been reported that M2 microglia membranes can repolarize M1 microglia to an M2 phenotype and secrete anti-inflammatory cytokines, functioning as a therapeutic agent [23].

Nanozymes have emerged as potential future therapeutics [24,25]. Manganese dioxide (MnO_2) nanoparticles, nanomaterial with exceptional enzyme-like catalytic capabilities, are widely used due to their simple production technique, low cost, high catalytic performance, and low environmental impact [26]. MnO_2 nanoparticles have been shown to react with low concentrations of H_2O_2 to create Mn^{2+} and O_2 [27,28]. They can also lower oxidative stress and inflammatory responses [29]. However, MnO_2 nanoparticles exhibit a degree of systemic toxicity and have a limited capacity to target disease locations [30]. Therefore, it is necessary to precisely deliver MnO_2 nanoparticles to the ischemic brain to efficiently restore injured neurons.

In this study, we developed M2-type microglia membranes-engineered Melatonin-loaded MnO_2 nanoparticles (M2-MnO_2/MT NPs) for the removal of various pathogenic components, including overproduced ROS and inflammatory microglia, providing a targeted therapy for ischemic stroke. The M2-type microglia membrane coating provides nanoparticles with intrinsic ischemia-homing and BBB-crossing capabilities. Moreover, the M2 microglia membranes can repolarize M1 microglia to an M2 phenotype and secrete anti-inflammatory cytokines, enhancing their therapeutic effect [23]. MnO_2 nanocrystals catalyze the decomposition of H_2O_2, reducing ROS levels and generating oxygen, which can alleviate hypoxia and further protect nerve cells in the ischemic brain. Melatonin (MT), a hormone released by the pineal gland with powerful antioxidant and free radical scavenging effects [31], was loaded into the MnO_2 nanoparticles *via* electrostatic interactions. The ROS-scavenging abilities of MT can mitigate the increase at ischemic locations. MT is also recognized as a crucial molecule in cellular physiology with protective effects on various cells and tissues, regulating inflammation and apoptosis in different pathophysiological situations [32,33]. In conclusion, the developed nano delivery system can reduce inflammation and protect neurons by reducing oxidative stress, which is a promising therapeutic option for the treatment of ischemic stroke.

Honeycomb-shaped MnO_2 nanospheres were synthesized using a modified soft chemistry approach [29,34]. In this method, oleic acid (OA) was employed to reduce $KMnO_4$ in distilled water at room temperature. OA served dual roles as both a reductant and a synthesis template, leading to the formation of MnO_2 core on the surface of the oil/water emulsions. Transmission electron microscope (TEM) images revealed that as-prepared MnO_2 nanospheres exhibited a honeycomb-like spherical morphology with an average diameter of approximately 160 nm (Fig. 1a). X-ray diffraction (XRD) analysis further characterized the MnO_2 nanospheres (Fig. S1 in Supporting information). Prominent XRD at (2θ) values of 12.25°, 24.48°, 36.76°, and 65.77° correspond to the (001), (002), (100), and (110) planes of K_xMnO_2 with a turbostratic structure [35]. MT was then added to the MnO_2 colloid solution and sonicated for 2 h to form MnO_2/MT nanoparticles (NPs). High performance liquid chromatography (HPLC) measurements indicated that the encapsulation efficiency and drug loading capacity of the MnO_2/MT NPs were 62.4 % and 23.8 %, respectively.

To obtain M2-polarized microglia membranes, BV2 microglial cells were incubated with interleukin 4 (IL-4) [36]. Flow cytometry confirmed that the M2 group expressed higher CD206 on the cell membrane surface compared to the M0 group when stimulated

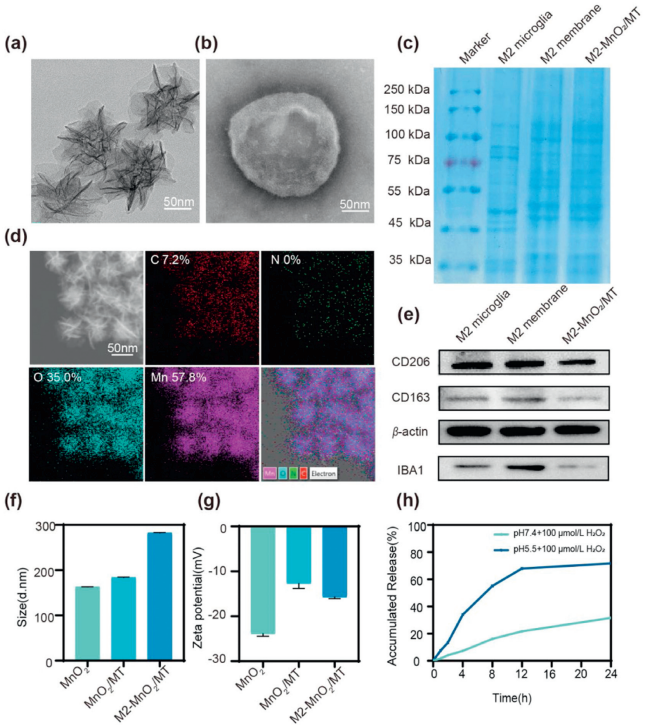


Fig. 1. The TEM images of (a) MnO_2 NPs and (b) M2-MnO_2/MT NPs. (c) SDS-PAGE electrophoresis analysis of proteins in M2 microglia, M2 membrane and M2-MnO_2/MT NPs. (d) The elemental mapping images of MnO_2 NPs. (e) Membrane surficial proteins in M2 macroglia, M2 membrane vesicles and M2-MnO_2/MT nanoparticles, analyzed with Western blot. Scale bar: 50 nm. (f) The size and (g) zeta potential of different samples ($n = 3$). (h) The release profile of MT *in vivo* from M2-MnO_2/MT NPs under conditions that mimic M1 microglia. Data are presented as means ± SD ($n = 3$).

with IL-4 (Fig. S2 in Supporting information). To enhance the stability and ischemia-homing capability of the nanoparticles, the isolated M2 microglia membrane was coated onto the surface of the MnO_2/MT NPs, resulting in M2-MnO_2/MT NPs. TEM images provided further evidence of successful membrane coating, showing a distinct shell surrounding the MnO_2 core (Fig. 1b). Sodium dodecyl sulfate-polyacrylamide gel electrophoresis (SDS-PAGE) analysis revealed that the protein profiles of the M2-MnO_2/MT NPs closely matched those of pure M2 microglia membranes (Fig. 1c), indicating the presence of membrane proteins on the nanoparticle surface. Additionally, Western blot analysis confirmed the presence of the M2 microglial-specific membrane protein (CD206, CD163 and ionized calcium binding adaptor molecule 1 (IBA1)) on the M2-MnO_2/MT NPs (Fig. 1e). Elemental mapping images obtained *via* energy-dispersive X-ray spectroscopy (EDS) demonstrated the elemental composition of the MnO_2 core, showing the presence of manganese (Mn), carbon (C), nitrogen (N), and oxygen (O) (Fig. 1d). Dynamic light scattering (DLS) and TEM were used to analyze the hydrodynamic size, zeta potential, and morphology of M2-MnO_2/MT NPs. DLS measurements showed that the M2-MnO_2/MT NPs had an average hydrodynamic diameter of approximately (Fig. 1f), indicating an increase in size due to membrane coating. The zeta potential decreased to −15.59 mV (Fig. 1g), suggesting successful surface modification with negatively charged M2 microglia membranes. The nanoparticles were well-formed and uniformly dispersed in the solution, as confirmed by the zeta potential and size distribution results. The M2-MnO_2/MT NPs were stable in 10 % fetal bovine serum (FBS) for 3 days (Fig. S3 in Supporting information), indicating the good colloidal stability of the M2-MnO_2/MT NPs in artificial physiological fluids.

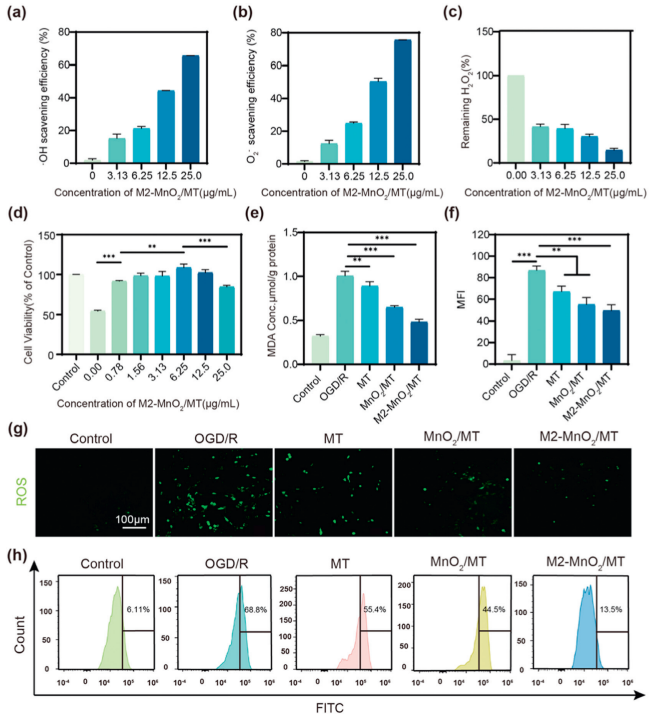


Fig. 2. ROS scavenging and antioxidative activity of M2-MnO_2/MT NPs. (a) $^{\bullet}OH$, (b) $^{\bullet}O^{2-}$, and (c) H_2O_2 scavenging ability of M2-MnO_2/MT NPs. (d) The cell viability of PC-12 cells after a treatment of 100 μmol/L $CoCl_2$ for 24 h and then treatments with various concentrations of M2-MnO_2/MT for 24 h. (e) The level of intracellular MDA after the administration of different NPs. $n = 3$. (g) Representative images of intracellular ROS levels found in PC-12 cells using DCFH-DA and (f) quantification of mean fluorescence intensity (MFI). $n = 3$. Scale bar: 100 μm. (h) Representative images of the intracellular ROS levels found in PC-12 cells by using Flow cytometry. Data are presented as the mean ± SD ($n = 3$). $^{**}P < 0.01$, $^{***}P < 0.001$.

Excessive production of ROS in ischemic regions leads to increased oxidative stress and creates an acidic microenvironment in the post-ischemic brain [37]. To simulate this environment, we investigated the drug release behavior of the M2-MnO_2/MT NPs at pH 5.5. Under normal physiological conditions (phosphate buffer saline (PBS), pH 7.4), the release of MT was minimal, with only about 10% released in the first 4 h. In contrast, at pH 5.5, the M2-MnO_2/MT NPs exhibited a significantly enhanced and accelerated release of MT, reaching near-complete release within 24 h (Fig. 1h). This acid-responsive release profile suggests that the nanoparticles can effectively release their payload in the acidic microenvironment of the ischemic brain, enhancing therapeutic efficacy. In summary, we successfully synthesized M2-MnO_2/MT nanoparticles with a core-shell structure, where the MnO_2/MT core is effectively coated with M2-polarized microglia membranes. The nanoparticles exhibit suitable size and surface charge for biomedical applications and demonstrate an acid-responsive release of MT, making them promising candidates for targeted therapy in ischemic stroke.

M2-MnO_2/MT NPs were successfully prepared and the safety of nanoparticles was investigated. Our cytotoxicity experiments revealed that M2-MnO_2/MT NPs were non-toxic at doses ranging from 0 to 6.25 μg/mL (Fig. S4 in Supporting information). Next, we tested their ability to scavenge various ROS, including $^{\bullet}OH$, $^{\bullet}O^{2-}$, and H_2O_2. The scavenging ability of M2-MnO_2/MT NPs increased when its concentration increased from 0 to 3.13, 6.25, 12.5 and 25 μg/mL, as illustrated in (Figs. 2a–c). The results showed that M2-MnO_2/MT could efficiently scavenge $^{\bullet}OH$, O^{2-}, and H_2O_2 and the scavenging ability all reached about 80% at 25 μg/mL. The remarkable antioxidant capabilities of M2-MnO_2/MT were proven.

Since one of the main factors leading to damage to brain cells is ROS, we next study the capacity of M2-MnO_2/MT NPs to scavenge various ROS within cells. Hypoxia inducible factor-1α (HIF-1α) and HIF-2α were significantly stabilized by $CoCl_2$ in normoxic circumstances. Compared to hypoxia-induced hypoxia and other hypoxia mimics, $CoCl_2$-pretreatment led to an increase in intracellular hypoxia levels, and HIF-1α and HIF-2α stabilization lasted for several hours [38]. PC-12 cells were treated with 100 μmol $CoCl_2$ to replicate neurons experiencing ischemia and reperfusion (Fig. S5 in Supporting information). We discovered that $CoCl_2$ induced considerable cell death in PC-12 cells; however, cell viability was recovered following treatment with MnO_2/MT and M2-MnO_2/MT NPs, particularly in the M2-MnO_2/MT NPs group (Fig. 2d). This finding indicates that M2-MnO_2/MT effectively restored PC-12 cells injured by $CoCl_2$. We also studied the cells' level of lipid peroxidation. We discovered that the malondialdehyde (MDA) content in cells was dramatically raised following $CoCl_2$-pretreatment damage and decreased after incubation with M2-MnO_2/MT NPs; there was a significant difference in the MDA content compared with the model group (Fig. 2e). We next employed the dichlorofluorescein diacetate (DCFH-DA) probe to determine the ability of M2-MnO_2/MT NPs to eliminate ROS from PC-12 cells. Treatment with 100 μmol/L $CoCl_2$ resulted in cellular shrinkage and increased intracellular ROS levels, as seen by an elevated green fluorescence signal (Figs. 2f and g). However, ROS levels were marginally reduced after MnO_2/MT NPs treatment, and ROS levels were significantly reduced in the M2-MnO_2/MT NPs group. As illustrated in Figs. 2f and g, the relative amount of ROS increased to 85% after 24-h treatment with 100 μmol/L $CoCl_2$. Compared with the group treated with $CoCl_2$ alone, the group treated with 6.25 μg/mL M2-MnO_2/MT exhibited a 30% reduction in the fluorescence intensity of ROS. Furthermore, flow cytometry data supported these findings (Fig. 2h and Fig. S6 in Supporting information). To further investigate the anti-apoptotic effect of M2-MnO_2/MT NPs, we found that apoptotic cells were significantly reduced in the M2-MnO_2/MT-treated group compared with the model group by TdT-mediated dUTP nick-end labeling (TUNEL) staining analysis (Fig. S7 in Supporting information).

The cellular uptake of MnO_2/MT and M2-MnO_2/MT NPs by PC-12 cells and human brain microvascular endothelial cells (HBMECs) was investigated using confocal laser scanning microscope (CLSM) (Figs. 3a and b and Fig. S8 in Supporting information). Cy5.5-labeled MnO_2/MT and M2-MnO_2/MT NPs were cultured with PC-12 cells and HBMECs for 2 h. MnO_2/MT NPs showed reduced cellular absorption compared to M2-MnO_2/MT NPs, obviously at both cells. Furthermore, we found that M2-MnO_2/MT NPs were rapidly taken up within 2 h. Confocal imaging also revealed that PC-12 cells absorbed M2-MnO_2/MT in a time-dependent manner.

The BBB is a key barrier to intracerebral drug delivery. It is necessary for therapeutic preparations to effectively cross the BBB and achieve full curative efficacy. To assess M2-MnO_2/MT NPs' ability to traverse the BBB, an *in-vitro* model was created. The *in vitro* BBB model was created using a 24-well transwell membrane with a pore size of 0.4 μm. HBMECs were seeded at a density of 5×10^4 cells/well and grown for 3 days. The upper HBMEC monolayer simulated the BBB barrier, whereas PC12 cells in the basolateral bottom represented intracerebral cells (Fig. 3c). The ability of M2-MnO_2/MT NPs to traverse the BBB was tested *in vitro* using CLSM. As we can see, M2-MnO_2/MT NPs exhibits higher penetration across the BBB than MnO_2/MT NPs (Fig. 3d). With increasing time, the ability of MnO_2/MT NPs and M2-MnO_2/MT NPs to penetrate the BBB increased. Moreover, we tested the capacity of M2-MnO_2/MT NPs to target the ischemic brain in stroke rats. The animal experiments have been reviewed and approved by the Ethics Committee of Shanghai University (ECSHU 2024–112). As shown in Fig. 3f and Fig. S9 (Supporting information), the fluorescence

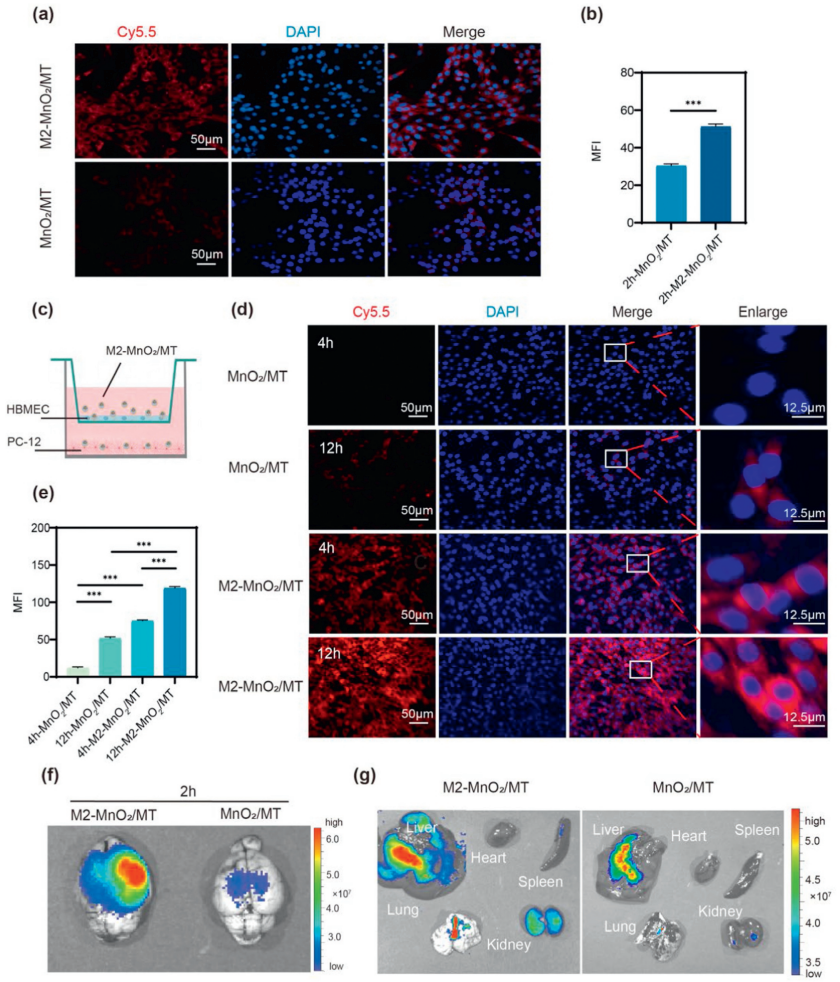


Fig. 3. (a) Uptake by HBMECs after coincubation with Cy5.5-labeled M2-MnO_2/MT NPs and MnO_2/MT NPs for 2 h and (b) quantitative statistical analysis. (c) Schematic illustration of the *in vitro* BBB model. (d) Uptake of M2-MnO_2/MT NPs and MnO_2/MT NPs by PC-12 cells as demonstrated by CLSM imaging at 4 and 12 h, and (e) quantitative statistical analysis of associated fluorescence by using Image J. (f) The targeting results of M2-MnO_2/MT NPs to the ischemic brain. The fluorescence intensity in the ischemic brain observed 2 h after the labeled nanoparticles were injected and (g) the main tissues after injection of labeled nanoparticles ($n = 3$). Results are reported as means ± SD ($n = 3$). $^{***}P < 0.001$.

signals in the brain of the Cy5.5-loaded MnO_2/MT NPs were relatively weak. Cy5.5-loaded M2-MnO_2/MT NPs treatment resulted in stronger signal, indicating the M2 microglial cell membrane innate inflammatory affinity and ability to target ischemia sites. Moreover, it indicates that M2-MnO_2/MT NPs reach the brain and are particularly abundant in the ischemic area. The distribution of NPs in different organs was examined, and it was demonstrated that the liver, spleen, and kidney were the metabolic organs where the nanoparticles were most found (Fig. 3g).

Next, we investigated the protective properties of M2-MnO_2/MT NPs against stroke *in vivo*. MACO mice were admi-nistrated with various groups (group 1: sham; group 2: saline; group 3: MT; group 4: MnO_2/MT NPs; group 5: M2-MnO_2/MT NPs) in accordance with the experimental procedure depicted in Fig. 4a. The *in vitro* hemolysis testing indicated that the rate of hemolysis was <5 % after treatment with all the investigated dose forms, meeting the criterion for drug hemolysis (Fig. S10 in Supporting information). Brains were removed after various treatments and stained with 2,3,5-triphenyltetrazolium chloride (TTC). The brain sections of the normal group were completely red, while the rat middle cerebral artery occlusion/reperfusion (MCAO/R) model group's infarcted area was predominantly white. Compared to the saline group, the M2-MnO_2/MT-treated group had a reduced cerebral infarction size (Fig. 4b). In addition, the cerebral infarct volume of the M2-MnO_2/MT NPs treated group also decreased from 37.5 % to 13.4 % (Fig. 4c). M2-MnO_2/MT NPs TUNEL assay was also conducted to confirm the therapeutic effects. We discovered that the fluorescence intensity of TUNEL labeling increased following ischemic stroke while TUNEL stained fluorescence intensity reduced after M2-MnO_2/MT NPs therapy, indicating less apoptosis and more neovascularization (Fig. 4d). We also examined astrocytes and microglia in the ipsilateral cortex, which are the two primary cell types that respond positively to the inflammatory response [39–41]. In M2-MnO_2/MT group, the amount of IBA1-labeled microglia and glial fibrillary acidic protein (GFAP)-labeled astrocytes were clearly reduced in ischemic brain (Figs. 4e–h), showing the anti-inflammatory effects of M2-MnO_2/MT NPs. M2-MnO_2/MT's outstanding ROS-scavenging activity may promote microglia polarization in the brain. Furthermore, compared to the control group, the level of IL-6 and tumor necrosis factor-α (TNF-α) in the brain tissue after being subjected to drug treatment were mostly reduced, reducing the inflammatory infiltration of the brain tissue (Fig. S11 in Supporting information). These results imply that M2-MnO_2/MT NPs can protect nerve cells from ischemic stroke and effectively accelerate the recovery of MCAO/R rats. Rat brain tissues were also subjected to Hematoxylin and Eosin staining (H&E) and Nissl staining 24 h after injection, and the outcomes were consistent with TTC staining (Fig. 4i). The cell morphology in the saline-treated

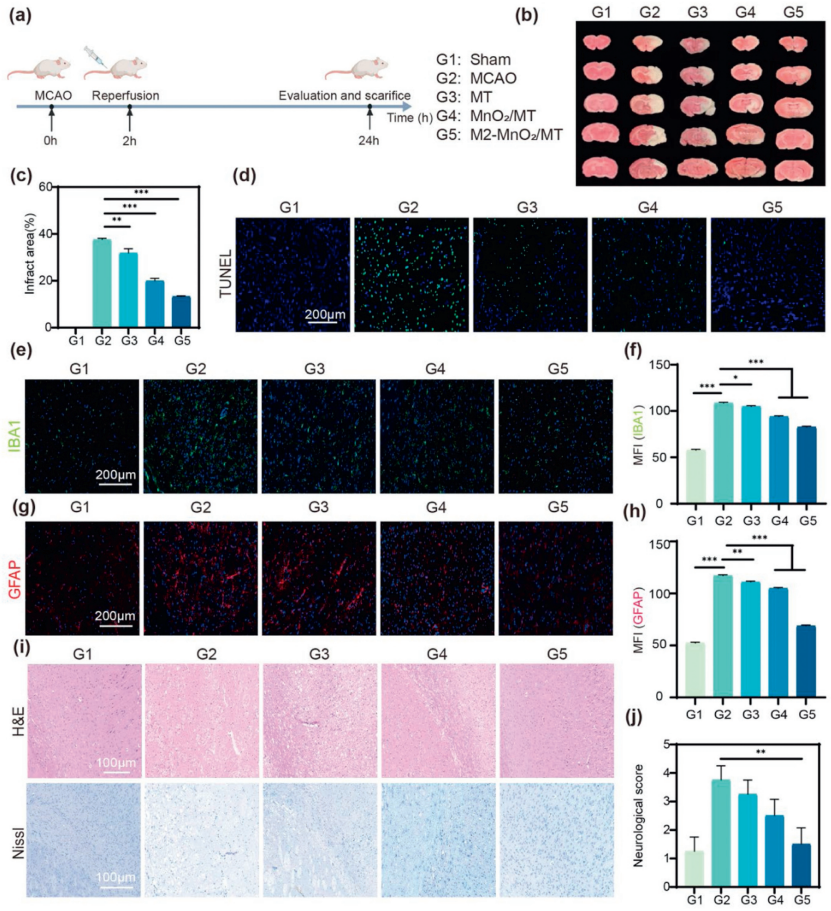


Fig. 4. (a) Schematic of the administration protocol. (b) Cerebral TTC staining of rats in different treatment groups and (c) quantification of TTC staining. $n = 3$. (d) TUNEL staining images (green: TUNEL; blue: 4′,6-diamidino-2-phenylindole (DAPI); scale bar: 200 μm) of brain tissue. (e) Immunofluorescence staining of IBA-1 (green). Scale bar: 200 μm. (f) Fluorescence quantification of (e). (g) Immunofluorescence staining of GFAP (red). Scale bar: 200 μm. (h) Fluorescence quantification of (g). Scale bar: 200 μm. (i) H&E staining and Nissl staining of the cerebral tissues of rats in different treatment groups. Scale bar: 100 μm. (j) Neurological score. Data are presented as the mean ± SD ($n = 3$). $^{*}P < 0.05$, $^{**}P < 0.01$, $^{***}P < 0.001$.

group differed greatly from that of the sham-operated group, since there was no intact cell structure. However, following MnO_2/MT and M2-MnO_2/MT NPs treatment, the cell morphology tended to resemble that of sham-operated group, demonstrating the developed nanoplatform has a good therapeutic effect on pathological abnormalities of cerebral ischemic stroke. The following neurological scores were also found using the Longa scoring criteria [42]. The neurological score in the M2-MnO_2/MT group decreased considerably (1 point, Fig. 4j) in comparison to the saline group (4 points).

Meanwhile, H&E staining of tissue sections revealed no major abnormalities, suggesting that intravenous distribution of nanomedicines did not result in any organ toxicity (Fig. S12 in Supporting information). M2-MnO_2/MT NPs did not result in an abnormal rise of alanine aminotransferase (ALT) or aspartate aminotransferase (AST) (Fig. S13 in Supporting information). These findings show that nanomedicines have a favorable safety profile.

In summary, we have developed an ischemia-homing nanozyme by integrating MT-loaded honeycomb MnO_2 nanoflowers with M2-type microglia membranes to rescue the ischemic penumbra in stroke. The M2-MnO_2/MT NPs exhibit acid-responsive properties, enabling on-demand drug release in the acidic microenvironment of ischemic brain tissue. The surface camouflage with M2-type microglial cell membranes imparts the intrinsic ischemia-homing and BBB-crossing capabilities to the biomimetic nanozymes. These nanozymes accumulate in the ischemic penumbra and rescue neurons by scavenging excess ROS, including $^{\bullet}OH$, $^{\bullet}O^{2-}$, and H_2O_2. They also modulate pro-inflammatory milieu by promoting the phenotypic transit of microglia from the pro-inflammatory M1 state to the anti-inflammatory M2 state. Our study demonstrates that the as-prepared M2-MnO_2/MT NPs significantly reduce cerebral infarct areas and provide substantial neuroprotection against ischemic stroke by lowering oxidative stress, inhibiting cell apoptosis, and decreasing inflammation. Preliminary safety assessments indicate that the use of M2-MnO_2/MT NPs does not exhibit acute toxicity; however, their long-term safety profile requires further investigation. Overall, the application biomimetic cell membrane-based nanozymes, as demonstrated in this study, may lead to new strategies for multitargeted stroke treatment and open new avenues for the therapy of cerebral diseases [43,44].

Declaration of competing interest

The authors declare that they have no known competing financial interests or personal relationships that could have appeared to influence the work reported in this paper.

CRediT authorship contribution statement

Chenchen Xie: Writing – original draft. **Jun Liao:** Writing – original draft. **Yi Li:** Writing – original draft. **Yunan Zhang:** Data curation. **Zhicheng Xiao:** Formal analysis. **Yun Wang:** Project administration. **Ting Chen:** Resources, Conceptualization. **Liyan Xiong:** Supervision. **Tao Pang:** Conceptualization. **Xiangao Jiang:**

Validation. **Feng Zhang:** Supervision, Resources. **Chuan Zhang:** Writing – review & editing, Supervision. **Tingfang Wang:** Methodology, Funding acquisition.

Acknowledgments

This work was supported by National Key R&D Program of China (No. 2022YFC3501700); National Natural Science Foundation of China (No. 82274059); Naval Military Medical University, Far East Talent Project (No. SL-33); and Talent Project established by Chinese Pharmaceutical Association Hospital Pharmacy department (No. CPA-Z05-ZC-2024–003); Shanghai Oriental Talent Plan Youth Program (formerly Shanghai Young Top-Notch Talent) (2023), the Baoshan District Medical Key Science (Specialty) and Specialty Brand Construction Project (No. BSZK-2023-A12).

Supplementary materials

Supplementary material associated with this article can be found, in the online version, at doi:10.1016/j.cclet.2025.110956.

References

[1] C.W. Tsao, A.W. Aday, Z.I. Almarzooq, et al., Circulation 147 (2023) e93–e621.
[2] A. Datta, D. Sarmah, L. Mounica, et al., Transl. Stroke Res. 11 (2020) 1185–1202.
[3] P. Jolugbo, R.A. Ariëns, Stroke 52 (2021) 1131–1142.
[4] J. Liao, L. Gong, Q. Xu, et al., Adv. Mater. 36 (2024) e2402445.
[5] J. Xu, A. Wang, X. Meng, et al., Stroke 52 (2021) 772–780.
[6] B. Wang, C. Wu, Z. Chen, et al., Acta Pharmacol. Sin. 42 (2021) 347–360.
[7] C.M. Gorick, V.R. Breza, K.M. Nowak, et al., Adv. Drug Deliv. Rev. 191 (2022) 114583.
[8] Z. Xiao, Y. Li, T. Chen, et al., Chem. Eng. J. 496 (2024) 154205.
[9] W. He, Q. Mei, J. Li, et al., Nano Lett. 21 (2021) 3033–3043.
[10] T. Tao, M. Liu, M. Chen, et al., Pharmacol. Ther. 216 (2020) 107695.
[11] W. Yu, E. Gong, B. Liu, et al., Chin. Chem. Lett. 34 (2023) 108205.
[12] Y. Dai, Y. Ding, L. Li, Chin. Chem. Lett. 32 (2021) 2715–2728.
[13] Y. Li, J. Liao, L. Xiong, et al., J. Control. Release 368 (2024) 607–622.
[14] Y. Pan, L. Li, N. Cao, et al., Biomaterials 314 (2025) 122852.
[15] Q. Huang, J. Liao, J. Li, et al., Chin. Chem. Lett. 36 (2025) 109914.
[16] I. Gottfried, N. Schottlender, U. Ashery, Biomolecules 11 (2021) 1520.
[17] J. Liao, L. Fan, Y. Li, et al., J. Control. Release 358 (2023) 439–464.
[18] T.V. Arumugam, J.W. Salter, J.H. Chidlow, et al., Am. J. Physiol. Heart Circ. Physiol. 287 (2004) H2555–H2560.
[19] G. Hu, Y. Su, B.H. Kang, et al., Nat. Commun. 12 (2021) 773.
[20] L. Li, C. Lenahan, Z. Liao, et al., Oxid. Med. Cell Longev. 2021 (2021) 6694566.
[21] D. Fu, Z. Wang, Y. Tu, F. Peng, Adv. Healthc. Mater. 10 (2021) 2001788.
[22] J. Shi, W. Yu, L. Xu, et al., Nano Lett. 20 (2019) 780–789.
[23] H. Ghuman, A.R. Massensini, J. Donnelly, et al., Biomaterials 91 (2016) 166–181.
[24] S. Wang, M. Cheng, S. Wang, et al., Adv. Mater. 36 (2024) 2403921.
[25] L. Ma, J.J. Zheng, N. Zhou, et al., Nat. Commun. 15 (2024) 233.
[26] H.Y. Xia, B.Y. Li, Y. Zhao, et al., Coord. Chem. Rev. 464 (2022) 214540.
[27] X. Yang, Y. Yang, F. Gao, et al., Nano Lett. 19 (2019) 4334–4342.
[28] W. Fan, W. Bu, B. Shen, et al., Adv. Mater. 28 (2015) 4155–4161.
[29] C. Li, Z. Zhao, Y. Luo, et al., Adv. Sci. 8 (2021) 2101526.
[30] L. Wang, M. Gu, X. Zhang, et al., Adv. Sci. 12 (2025) 2413367.
[31] M. Yao, P.m. Pu, Z.y. Li, et al., J. Pineal Res. 74 (2023) e12859.
[32] J. Liao, Y. Li, Y. Luo, et al., Mol. Pharm. 19 (2022) 3026–3041.
[33] L.C. Ku, M.L. Sheu, H.H. Cheng, et al., Biomed. Pharmacother. 161 (2023) 114476.
[34] J. Liao, Y. Li, L. Fan, et al., ACS Nano 18 (2024) 5510–5529.
[35] W. He, Q. Mei, J. Li, et al., Nano Lett. 21 (2021) 3033–3043.
[36] Y. Song, Z. Li, T. He, et al., Theranostics 9 (2019) 2910.
[37] Y. Lu, C. Li, Q. Chen, et al., Adv. Mater. 31 (2019) 1808361.
[38] P. Prasad, C.R. Gordijo, A.Z. Abbasi, et al., ACS Nano 8 (2014) 3202–3212.
[39] S.A. Liddelow, K.A. Guttenplan, L.E. Clarke, et al., Nature 541 (2017) 481–487.
[40] J. Wu, W. Yin, Y. Zhang, et al., Chin. Chem. Lett. 31 (2020) 1881–1886.
[41] International Multiple Sclerosis Genetics Consortium, Science 365 (2019) eaav7188.
[42] J. Muñoz-Sánchez, M.E. Chánez-Cárdenas, J. Appl. Toxicol. 39 (2019) 556–570.
[43] W. He, Z. Zhang, X. Sha, Biomaterials 277 (2021) 121111.
[44] Y. Chong, J. Ning, S. Min, et al., Chin. Chem. Lett. 33 (2022) 3315–3324.